Applied Thermal Engineering 279 (2025) 127617

Contents lists available at ScienceDirect

Applied Thermal Engineering

journal homepage: www.elsevier.com/locate/apthermeng

Research Paper

Energy-efficient polymer/bitumen roofing materials formulated with non-encapsulated beeswax phase change material

E. Álvarez-Gallardo, A. Tenorio-Alfonso, A.A. Cuadri *

Pro2TecS-Chemical Process and Product Technology Research Centre, Department of Chemical Engineering, ETSI, Campus de "El Carmen", Universidad de Huelva 21071 Huelva, Spain

ARTICLE INFO

Keywords:
Energy-efficient roofing materials
Thermal energy storage
Beeswax
Bio-based PCMs
Indoor thermoregulation tests
Energy saving

ABSTRACT

With the aim of overcoming the drawbacks involved in PCM encapsulation and taking into account the potential of beeswax as bio-PCM, the main objective of this work is to develop novel energy-efficient roofing materials for building applications by its direct inclusion. These materials are formulated with bitumen (B), styrene butadiene styrene copolymer (SBS) and beeswax (BW) as bio-based phase change material. To that end, the effects of possible interactions between B compounds and BW on thermal storage capacity and technological characterization were firstly evaluated on binary B/BW blends. Afterwards, leakage tests conducted on ternary B/SBS/BW blends revealed that form-stable materials (with no BW leakage) can be manufactured with a maximum BW concentration of 30 wt%. Thus, the prototype roofing material composed of 61.6 wt% B, 8.4 wt% SBS and 30 wt % BW shows excellent thermal stability (no weight loss up to ca. 200 °C) and meets the technological requirements specified by ASTM D8051 for wax-modified asphaltic roofing products. In addition, the selected roofing material displays high thermal storage capacity (ca. 50 J/g) for a long period of time (at least, for 300 heating/cooling cycles), which is reflected in the results derived from the indoor thermoregulation tests conducted in a climatic chamber. Interestingly, the tests conducted on a reduced-scale isolate room indicated a percentage reduction in the heat needed to be removed from the room of 9.3 % when comparing the prototype roofing material with the commercial SBS bituminous binder.

1. Introduction

Energy consumption in buildings accounts for 30 % of the world's total and is also responsible for approximately 40 % of the total CO_2 emissions [1]. Globally, the energy consumed for space heating and cooling is as high as 40 % and 61 % out of the total energy demand in commercial and residential buildings, respectively [2,3]. Considering these facts, it becomes obvious that the solution lies on the development of energy-efficient building materials. In this context, thermal energy storage (TES) based on latent heat phase change materials (PCMs) is emerging as an efficient approach for reducing greenhouse gas emissions, and the energy consumption in buildings by improving the ability to manage its thermal environment [4]. Thus, the PCM included in the building envelope stores the solar energy available during the day by changing from solid to liquid phase and, therefore, minimizing the heat that enters from the outside. The same PCM helps to maintain thermal comfort during the night when the outside temperature is lower than phase change temperature by changing its phase back to solid [5]. However, a critical issue pertaining to these solid-to-liquid PCMs is the leakage of liquid after melting temperature. To solve this, the encapsulation of PCMs inside a protective shell material is the most common solution. However, this approach has some drawbacks that would restrict its industrial applications [6], including the high cost of the procedure and the daunting task of selecting and developing the appropriate materials for the application [7].

A significant number of recent publications with satisfactory results can be found in the literature exploring the incorporation of PCMs in different building components like walls, floor, roof, cement, windows, etc. [8–12]. From them, it can be stated that paraffin PCMs dominate the market for PCMs in buildings due to their stability, ease of encapsulation, good recyclability and abundance [13]. However, paraffin PCMs (which are produced from petroleum products) have some significant disadvantages as high cost, large environmental impacts, and significant social and health risks of production [14]. Consequently, research needs to be conducted on developing TES materials from renewable feedstocks or bio-based PCMs with high thermal properties that are cost-effective for application in buildings. In this sense, products obtained from

* Corresponding author.
E-mail address: antonio.cuadri@diq.uhu.es (A.A. Cuadri).

https://doi.org/10.1016/j.applthermaleng.2025.127617
Received 21 May 2025; Received in revised form 1 July 2025; Accepted 17 July 2025
Available online 17 July 2025
1359-4311/© 2025 The Author(s). Published by Elsevier Ltd. This is an open access article under the CC BY license (http://creativecommons.org/licenses/by/4.0/).

Nomenclature

B	Bitumen
BW	Beeswax
T	Temperature [°C]
P	Penetration value [1/10 mm]
t	Time [min]
Q	Heat [J]
m	Mass [kg]
Cp	Specific heat capacity [J/(kg·K)]

Greek letters

ΔH	Enthalpy of phase change [J/g]
η	Relative enthalpy efficiency
Ω	Percentage reduction in the heat needed to be removed from the room [%]

Subscript

m	Melting
c	Crystallization
o	Onset of the phase change
p	Peak of the phase change
up	Uppermost surface of the roofing material
lo	Lowermost surface of the roofing material
su	Surrounding air
in	Inside the isolated room
R&B	Ring and ball softening
de	Desired indoor
air	Air

Acronyms

SBS	Styrene butadiene styrene copolymer
TES	Thermal energy storage
PCM	Phase change material
TGA	Thermogravimetric analysis
DSC	Differential scanning calorimetry
XPS	Extruded polystyrene
LDPE	Low-density polyethylene
SEBS	Styrene-b-(ethylene-co-butylene)-b-styrene

plants or animals like margarine [15], coconut [16,17], coffee oil [18], soya oil [19,20], palm oil [21–23], beeswax [24,25] or beef tallow [26] were studied as bio-based PCMs in the manufacture of building materials. Among them, beeswax stands out for its large thermal heat storage capacity (ca. 175 kJ/kg) when compared to other bio-based PCM or industrial semi-crystalline polymers such as polyester [24]. In addition, beeswax presents a wide melting process centered at ca. 60 °C [5], which makes it a suitable bio-PCM for use as roofing materials for warm climates [25]. Importantly, beeswax is not digestible by humans, which, in conjunction with its non-toxicity, chemical stability and biodegradability turn into an eco-conscious PCM alternative to replace petroleum based paraffin PCM [27,28]. Some recent papers have developed thermal energy storage materials including beeswax as bio-PCM. Belgacem et al. [24] prepared different blends of beeswax with low-density polyethylene (LDPE) or styrene-b-(ethylene-co-butylene)-b-styrene (SEBS) as supporting materials to prevent beeswax leakage. Rathore et al. [25] synthetized different composites from beeswax, bentonite clay as supporting material, and graphite powder as additive to increase the thermal conductivity. These papers were limited exclusively to an in-depth microstructural and thermal characterization of the proposed materials. However, no indoor thermoregulation tests were carried out to assess their potential application as thermal energy storage materials in buildings.

Therefore, in order to overcome the drawbacks involved in PCM encapsulation and taking into account the potential of beeswax as bio-PCM, the main objective of this work is to develop novel energy-efficient roofing materials for building applications by its direct inclusion. These materials are formulated with bitumen, styrene butadiene styrene (SBS) triblock copolymer (a polymer typically used in roofing industry) as supporting material and beeswax (acting as bio-based PCM). Bitumen, a by-product from crude oil distillation, has been widely used in roofing and waterproofing membranes for building applications due to its suitable properties (superior waterproof, adhesive properties, low cost, etc.) [13,29]. The bitumen modification by SBS has been widely used in roofing industry to manufacture bituminous binders with enhanced thermomechanical properties. This fact is ascribed to the creation of a continuous SBS-rich phase throughout the binder, which appears for binders containing 5–7 wt% SBS [30,31]. Thus, it is expected that this created SBS network will be capable of retaining a significant amount of beeswax without leakage. In fact, in a previous paper [32], it was found that a binder formulated with 8.4 wt% SBS retained 30 wt% commercial paraffin-wax without leakage. Thus, manuscript structure was divided into three steps: i) considering that non-encapsulated beeswax PCM was used, the effects of possible interactions between bitumen compounds and beeswax on microstructure, heat storage capacity and technological characterization were firstly evaluated on binary bitumen/beeswax blends; ii) ternary bitumen/SBS/beeswax blends at a fixed bitumen/SBS mass ratio (equivalent to the commercial 12 wt% SBS bitumen binder [30]) were manufactured, and the maximum beeswax concentration to obtain form-stable (no PCM leakage) binders was determined by leakage tests (according to EN 13301); and iii) a comprehensive thermal energy storage characterization was conducted on the selected ternary form-stable binder to evaluate its thermal stability, thermal storage capacity and thermal reliability. The results derived from this research open up new opportunities for the development of novel energy-efficient roofing materials for building applications by using non-encapsulated bio-PCMs.

2. Experimental

2.1. Materials

The bio-based PCM used in this study was beeswax (referred to as BW), supplied by Sigma-Aldrich (Spain), with a melting temperature around 60 °C. BW is a natural, hydrophobic and biodegradable wax produced in the beehive by honeybees [24]. A SBS (styrene butadiene styrene) triblock copolymer containing 31 wt% styrene (trade name C501), provided by Dynasol (Spain), was employed as bitumen modifying agent. A base bitumen (referred to as B), with penetration grade within the range 40/50, was also used for the manufacture of the bituminous roofing materials.

2.2. Sample preparation

Binary blends of B with 10, 20, 30 and 40 wt% BW were prepared in a Silverson L5 Laboratory mixer, using a general-purpose disintegrating head, at 150 °C with an agitation speed of 3500 rpm for 15 min (according to processing protocol A)) illustrated in Fig. 1). Thus, for binary blends, a processing temperature of 150 °C was selected. At this temperature, the BW is molten and the bitumen is soft enough to obtain homogeneous binder after 15 min at an agitation speed of 3500 rpm. In addition, this processing temperature is below the initial thermal degradation of BW (~200 °C).

In addition to that, another reference binary blend of B and 12 wt%

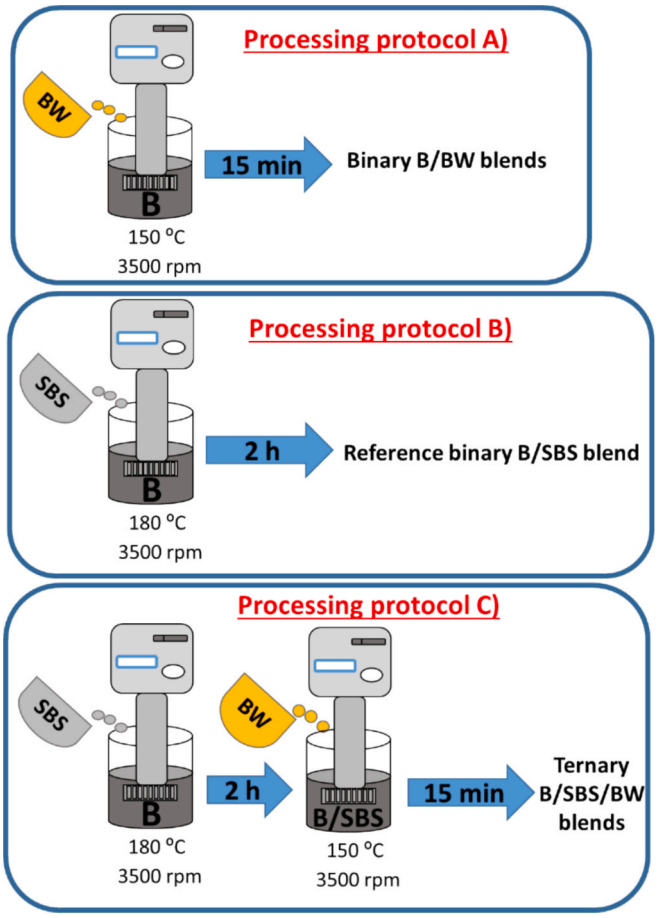

Fig. 1. Different processing protocols used to manufacture the bituminous materials.

SBS (usual formulation used in the roofing industry [30]) was also processed with the same mixer following the processing protocol B). In the case of SBS/bituminous binder, it is well known that a combination of high processing temperature (170–180 °C), high processing time (1.5–2 h) and high shear is required to create the continuous SBS-rich phase [31].

Finally, ternary bituminous blends containing B, SBS and BW were prepared at a fixed B/SBS mass ratio of 7.33, which corresponds to the reference B/SBS binder containing 12 wt%. In a previous paper [32], it was found that a bituminous binder with a B/SBS mass ratio of 7.33 retains 30 wt% commercial paraffin wax without leakage. Based on these results, two ternary blends were formulated with 30 and 40 wt% BW with respect to the total binder mass. These ternary B/SBS/BW were processed according to the protocol C) displayed in Fig. 1. Firstly, SBS was added to bitumen at the processing parameters commented above (180 °C, 2 h, 3500 rpm) to create the continuous SBS network throughout binder; afterwards, the corresponding amount of BW was added until homogenous binders were obtained. The idea was to first create the continuous SBS network throughout the binder and then finish the processing with the beeswax addition.

The nomenclature and composition of all samples considered in this study are gathered in Table 1.

Finally, it is worth noting that two samples were prepared for each formulation.

2.3. Tests and measurements

2.3.1. Technological tests

Ring-and-ball softening temperature and penetration measurements (two technological tests typically used for bitumen characterization) were carried on bituminous samples following EN 1427 and 1426 standards, respectively. More details on the measurement procedure for both tests can be found in the Supporting Information. Three replicas were recorded for each sample.

Table 1
Nomenclature and composition of all samples.

Nomenclature	Bitumen (wt.%)	SBS (wt.%)	B/SBS (wt.%/wt.%)	Beeswax (wt.%)
B	100	0	–	0
BW	0	0	–	100
B/BW10	90.0	0	–	10
B/BW20	80.0	0	–	20
B/BW30	70.0	0	–	30
B/BW40	60.0	0	–	40
B/SBS	88.0	12	7.33	0
B/SBS/BW30	61.6	8.4	7.33	30
B/SBS/BW40	52.8	7.2	7.33	40

2.3.2. Thermogravimetric analysis test

Thermogravimetric analysis (TGA) tests were conducted in a TA Q-50 (TA Instruments, USA). Temperature sweeps (10 °C·min^{-1}; from 30 to 550 °C) were carried out on 5–10 mg samples of pure components and bituminous blends under nitrogen atmosphere. Two replicas were recorded for each sample.

2.3.3. Leakage tests

Leakage tests were performed on ternary B/SBS/BW samples according to EN 13301 standard. To that end, a portion of bituminous binders (1.7 g) in a ring (16 mm internal diameter) were put on a piece of filter paper (with thickness of 2.0 mm) and then placed in an oven at a constant temperature of 80 °C (temperature higher than BW melting temperature) for 5 days. Afterwards, the leakage rate (L) is calculated as the arithmetic mean of the four measurements of the exudate circle (each 45°) minus the inner diameter of the ring (16 mm) and divided by 2. In order to explore the effects of repeated heating/cooling cycles on leakage rate, 10 g of sample was placed in an oven at 80 °C for 30 min and then allowed to cool for another 30 min at room temperature. This heating/cooling cycle was repeated 100 times. After that, sample was subjected to the leakage test. Three rings were used for each bituminous binder.

2.3.4. Optical microscopy

Optical microscopy was used to explore the microstructure of the samples by means of an Olympus BX51 (Japan) microscope coupled to an LTS-350 Heating-Freezing Stage controlled by a Linkam TP94 (Linkam Scientific Instruments, UK). A small amount of ternary bituminous binder was placed on standard microscope slides (76 × 26 mm) and heated up to 100 °C for 10 min on a Heating-Freezing Stage. Afterwards, samples were cooled down at the controlled rate of 1 °C/min for observation at 25 °C under or without crossed polarisers.

2.3.5. Differential scanning calorimetry analysis

Differential Scanning Calorimetry (DSC) was performed with a Q-250 DSC (TA Instruments, USA). Tests were carried out under N_2 atmosphere at a flow rate of 50 mL min^{-1} using 10–20 mg samples sealed in hermetic aluminium pans. In order to ensure the same recent thermal history, samples were subjected to the following procedure: (a) a first rapid heating ramp to 80 °C to remove the thermal history of the samples, (b) a cooling ramp to −25 °C at 10 °C/min and kept at this temperature for 10 min and, (c) a second heating ramp to 80 °C at 10 °C/min. To explore the thermal reliability of the ternary B/SBS/BW binders, (b) and (c) scans were repeated 300 times. The onset temperature for the melting ($T_{m,o}$) or crystallization ($T_{c,o}$) process of the PCM was calculated from the point of maximum slope of the leading side of the transition

peak and extrapolating the heat flow base line on the same side; the temperature peak for the melting ($T_{m,p}$) or crystallization ($T_{c,p}$) process was the temperature at which the largest deviation of the heat flow signal form the virtual baseline is measured; and the enthalpy of the phase change for the melting (ΔH_m) or crystallization (ΔH_c) process was calculated as the area under the peak by numerical integration. Three replicas were recorded for each sample.

2.3.6. X-ray diffraction measurements (XRD)

The crystalline structure of beeswax and bituminous binders were analysed using a D8 Advance X-ray diffractometer (Bruker-AXS, Germany) at room temperature (25 °C). The X-ray diffraction pattern was obtained under the following instrumental conditions: 30 mA, 40 kV, angle 2θ: 3° and 40°, step size = 0.02°. A copper Kα/K target (λ = 1.54) was used for the generation of the X-rays. All the samples were prepared by placing a small amount on a supporting glass slide of 25 × 25 mm^2, which was heated over beeswax melting temperature (130 °C) to flatten and obtain approximately 1 mm-thick film followed by cooling to room temperature. Afterwards, the sample-containing slide was located at the centre of a metal holder, externally shaped to be allocated in the instrument.

2.3.7. Fourier transform infrared spectroscopy (FTIR)

Fourier transform infrared spectroscopy (FTIR) spectra of beeswax and bituminous binders were obtained. To that end, firstly, a weight of 0.7 g of sample was dissolved in 25 mL dichloromethane. Afterwards, the resultant solution was laid on a potassium bromide disk (32 × 3 mm), which was subsequently exposed to ambient for removing solvent via evaporation. Finally, the KBr disk was placed into the sample holder and the FTIR spectra were obtained in a wavenumber range of 400–4000 cm^{-1}, at 4 cm^{-1} resolution, in the transmission mode.

2.3.8. Thermomechanical properties

The thermomechanical characterization of bituminous binders was conducted in a SmartPave 102e rheometer (Anton Paar, Austria), and consisted of temperature sweep tests in oscillatory shear. Measurements were conducted at 10 rad/s, from 30 to 80 °C, at a heating ramp of 2 °C/min, and using a plate-plate geometry (25 mm diameter and 1 mm gap). Tests were carried out at strains values within the linear viscoelastic region (LVR). Two replicas were recorded for each sample.

2.3.9. Density and thermal conductivity

The density, at 25 °C, of bituminous binders was measured according to EN 15326 standard. Three replicas were recorded for each sample.

The thermal conductivity, at 45 °C, was measured using the non-destructive Transient Hot-Bridge (THB) technique by a THB 100 device from Linseis GmbH (Germany). A sensor type A with a metal frame (A-13890) was used for the measurements. The sensor was placed between two equal flat faces of two samples (minimum sample size, 20 × 40 × 5 mm) of the same formulation and thermostatized in a lab Heratherm oven (Thermo Scientific, Germany). Ten replicas were recorded for each sample.

2.3.10. Indoor thermoregulation tests in the climatic chamber

To conduct the thermoregulation performance, a reduced-scale isolated room (0.23 × 0.19 × 0.19 m) was built by using 50 mm thick extruded polystyrene (XPS, with a thermal conductivity of 0.030 W/m°C) foam walls with a bubble insulation foil to cover at the bottom and the four lateral sides (Fig. S1A of the Supporting Information). The top side was covered by one of the bituminous binders (0.11 × 0.11 × 0.01 m) acting as roofing materials for each experiment. The mockup was placed in a climatic chamber (FDM Environment Makers, model 40T180V150PRO, see Fig. S1B of the Supporting Information) equipped with a solar simulator (halogen lamp) and a controlled temperature compartment (0.45 × 0.55 × 0.60 m). In addition, different temperature sensors were used to monitor temperature variations in the uppermost and lowermost surface of the roofing material (referred to as T_{up} and T_{lo}, respectively), the temperature of the surrounding air (T_{su}), and the air temperature inside the isolated room (T_{in}). For each experiment, T_{su} was kept at 27.5 ± 1.0 °C and the roofing material was subjected to an incident radiation of 1000 ± 25 W/m^2 for 90 min. Temperature sensors were connected to a dataTaker DT80-AL (Thermo Fisher Scientific Australia Pty Ltd) data logging instrument for temperature data recorder every 20 s, which was in turn connected to the computer via USB port. A scheme of this experimental setup is sketched in Fig. 2. More details about the indoor thermoregulation tests can be found in the Supporting Information.

2.3.11. Statistical analysis

The data were reported as means ± standard deviation statistically assessed by analysis of variance (ANOVA, $p < 0.05$) by means of the statistical package included in OriginPro software.

3. Results and discussion

3.1. Microstructural characterization

The knowledge of the crystalline structure of bituminous materials is of vital importance for their final application, because it is directly linked to the energy storage capacity since a large crystallinity will result in high phase change enthalpy. To that end, Fig. 3 displays the wide-angle XRD patterns of beeswax (BW), binary B/SBS sample (B/SBS) and ternary B/SBS/BW30 blend.

With regard to pristine beeswax, the XRD pattern is characterised by two well-defined peaks located at 2θ = 21.5 and 23.9°, which are ascribed to interplanar spacing of ordered molecules, pointing out its crystalline state [24,33,34]. As for binary B/SBS binder, no characteristic peak was detected in the 2θ interval considered. Interestingly, the ternary B/SBS/BW30 binder exhibits the above-commented peaks attributed to beeswax at the same positions, but with lower intensity proportional to beeswax content in the sample. Therefore, these results indicate that the internal crystal structure of beeswax was not affected during sample preparation.

In addition, it is well known that any PCM must be inert with the supporting material that holds it [35]. Thus, aiming to explore possible chemical interactions, Fig. 4 shows FTIR spectra, between 400 and 4000 cm^{-1}, for BW, binary B/SBS sample and ternary B/SBS/BW30 blend.

With regard to BW, it can be viewed that infrared signals due to symmetric stretching and asymmetric stretching of CH and CH_2 aliphatic hydrocarbons can be seen at 2916 and 2848 cm^{-1}. The peaks at 1739 and 1207 cm^{-1} correspond to presence of C═O ester fatty acid group. Additionally, the band at 730 cm^{-1} is indicative of the rocking vibration in the plane of the CH_2 group [24,25,34].

As for binary B/SBS binder, the bands due to the aliphatic CH stretching vibration (2916 and 2848 cm^{-1}) are also observed. The broad band within the 3730–3016 cm^{-1} region is attributed to the stretching vibration of –OH. The aromatic C═C stretching vibrations are located at 1634 cm^{-1}. The C–H bonds found at 1459 cm^{-1} proved to be asymmetric deformation in CH_2 and CH_3, and the C–H bonds noticed at 1374 cm^{-1} are ascribed to the symmetric deforming in CH_3 vibrations. The 966 cm^{-1} peak arises from C–H out-of-plane bending in *trans*-alkene groups, which is part of the most common polybutadiene structure of SBS [13,14,19,36].

Interestingly, new bands are not detected in the FTIR spectrum for the ternary B/SBS/BW30 binder, and only changes in its areas are noticed. This results suggests the absence of chemical interactions between the different constituents of the ternary binder.

3.2. Thermal storage capacity and technological characterization of binary blends

The main goal of this paper was to manufacture form-stable roofing

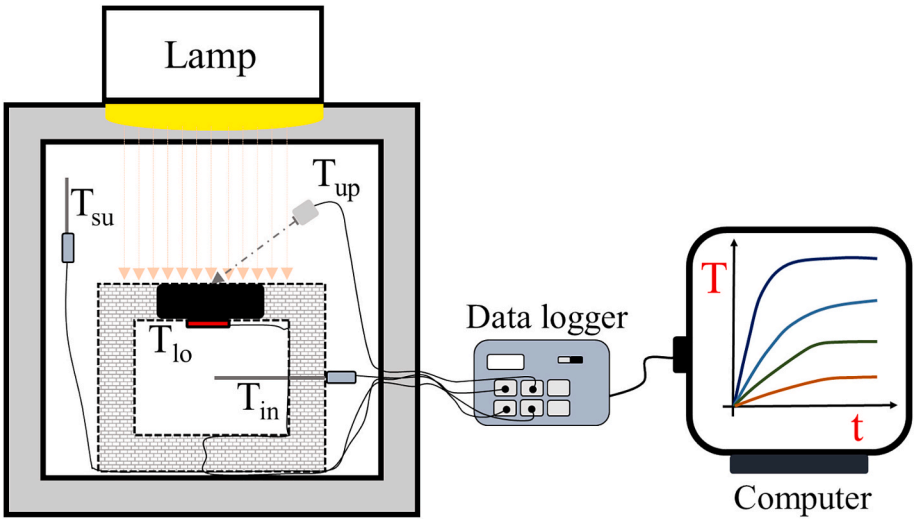

Fig. 2. Scheme of the experimental setup used for the indoor thermoregulation tests.

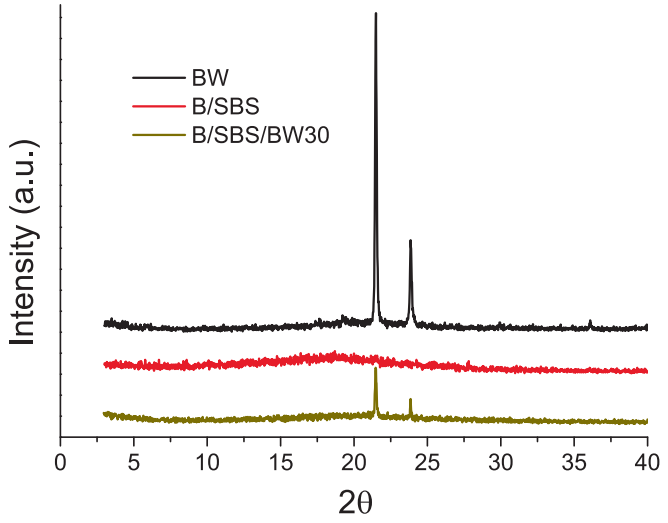

Fig. 3. XRD patterns of beeswax, binary B/SBS and ternary B/SBS/BW30 blends.

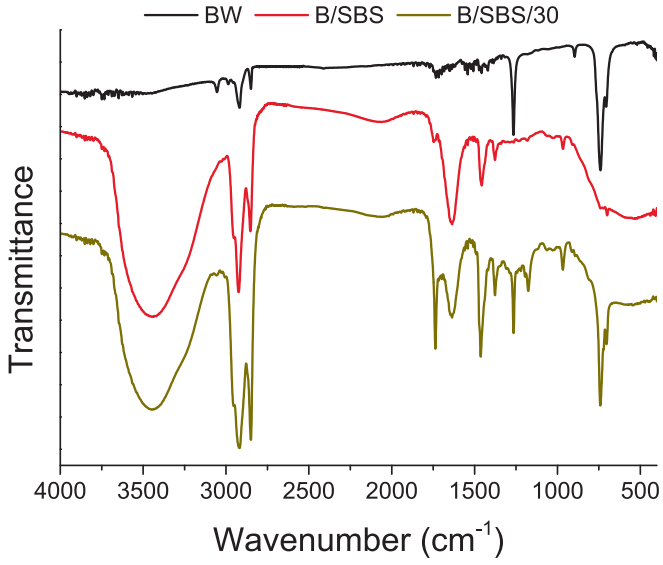

Fig. 4. FTIR spectra, from 400 to 4000 cm^{-1}, for beeswax, binary B/SBS and ternary B/SBS/BW30 blends.

bituminous materials with improved thermal energy storage features using non-encapsulated PCM (in this case, beeswax). Thus, taking into account that bitumen is a complex material, the effects of possible interactions between bitumen compounds and beeswax on the heat storage capacity will be assessed first. To that end, Fig. 5 shows heating/cooling DSC scans of base bitumen (B), beeswax (BW) and their corresponding binary B/BW blends.

Whereas B sample does not exhibit any thermal events in the temperature range studied, BW displays wide asymmetric endothermic and exothermic peaks mainly ascribed to the melting (during heating scan) and crystallization (in the cooling cycle) of its crystalline structures. The broad melting/crystallization peaks are related to the presence of mixtures of molecules with different lengths and melting points [37]. In addition to that, the signal asymmetry indicates the presence of other overlapped thermal events, as can be seen in Fig. 5 by the splitting of melting/crystallization peak. Thus, an additional peak during the heating or cooling scan just below the peak ($T_{m,p}$ and $T_{c,p}$ values in Table 2) is attributed to solid–solid or polymorphic phase transitions due to the movement of the material into its initial rotator phase [25,37,38].

As for BW sample, Table 2 gathers its melting ($T_{m,p}$) and crystallization ($T_{c,p}$) peak at 63.04 and 56.14 °C, respectively, with enthalpy values (ΔH_m and ΔH_c) of 175.68 and 176.66 J/g. Interestingly, this large thermal heat storage capacity makes beeswax a cost-effective bio-based PCM with excellent thermal energy storage properties. With regard to binary B/BW blends, the BW melting/crystallization events are shifted to lower temperatures as BW concentration in the blend decreases. This fact is due to morphological influences consequence of thermodynamically favourable interactions between components in the blend (e.g., variations in lamellar thickness, degree of crystalline perfection or properties of the amorphous phase surrounding the crystalline phase). As was reported for bitumen/paraffin wax blends [39–41], this effect is ascribed to the formation of crystallites with smaller sizes due to a partial compatibility between some bitumen compounds and paraffin crystalline structures. Similarly, some crystallizable maltenic molecules naturally present in bitumen (most probably waxes and saturates) could diffuse to the BW-rich structures leading to modifications in its crystalline phase. Nevertheless, binary B/BW blends display thermal storage capacity within a temperature range suitable for solar energy applications as roofing materials (from ca. 35 to 60 °C) [42,43]. In addition, the ability of a bituminous blend to retain the BW latent heat can be assessed by the relative enthalpy efficiency (η), which is calculated as follows:

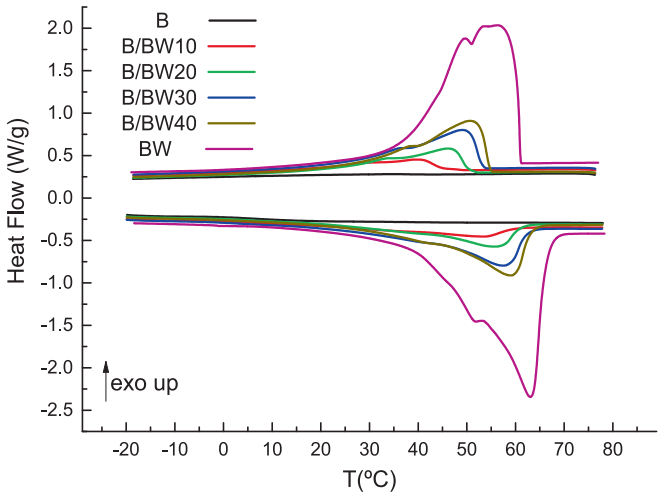

Fig. 5. DSC heating and cooling scans of bitumen, beeswax and their binary B/BW blends.

$$\eta = \frac{\Delta H_{m,blend}}{\Delta H_{m,BW} \cdot w_{BW}} \cdot 100 \quad (1)$$

where $\Delta H_{m,blend}$ is the melting enthalpy of the bituminous blend, $\Delta H_{m,BW}$ is the melting enthalpy of pristine beeswax, and w_{BW} corresponds to the weight content of beeswax in the blend. As can be observed in Table 2, binary B/BW blends show η values around 96 %, indicating that most of the crystalline structure of BW is retained in the blends and, thereby the latent heat capacity of BW is only weakly reduced.

Once the thermal storage capacity of binary B/BW binders was studied, the effects of BW concentration on the technological characterization is now considered. On the one hand, the high temperature performance of binary blends was evaluated by means of ring-and- ball softening temperature ($T_{R\&B}$) tests. Thus, as can be observed in Fig. 6A and Table 2, $T_{R\&B}$ values are strongly correlated with the melting process of the BW-rich phase and points out that the major softening happens at temperatures just above the DSC melting peak temperature ($T_{m,p}$ values in Table 2). Thus, pristine BW presents a $T_{R\&B}$ of 67.8 °C, which is only slightly higher than its melting peak ($T_{m,p}$ value of 63.0 °C). Similar trend is detected for bituminous B/BW blends, with $T_{R\&B}$ values ranging from 53.5 °C, for base bitumen, up to 63.5 °C for B/BW40 sample.

On the other hand, the consistency of the sample at 25 °C (temperature below BW melting process) can be evaluated by penetration (P) values, with lower P values being measured as sample stiffens. As seen in Fig. 6B, the decrease in P values with increasing BW concentration in binary blends is consistent with the presence of a highly-crystalline BW-rich phase which is much harder than the bituminous phase (with P values of 9 and 43 1/10 mm for pristine BW and base bitumen, respectively). Even though higher BW content results in binary B/BW blends with larger thermal storage capacity, there are two main reasons why these blends cannot be used in roofing applications: (a) on the one hand, the use of non-encapsulated beeswax as PCM in the binary blends makes its leakage unavoidable when $T_{R\&B}$ is exceeded, and (b) the International Standard ASTM D8051 for wax-modified asphaltic products intended for use in roofing applications demands $T_{R\&B}$ values between 99 and 110 °C (striped area in Fig. 6A), which are much higher than those measured for binary B/BW blends. To solve them, the inclusion of a polymer typically used in roofing industry (styrene butadiene styrene (SBS) triblock copolymer) in the blend formulation allows us to manufacture form-stable roofing materials that also meet the technological specifications.

3.3. Thermoregulation performance of a prototype roofing material

As commented above, one of the goals of adding SBS in the blend formulation is to avoid the beeswax leakage. For this purpose, leakage tests according to EN 13301 were conducted on ternary blends formulated with 30 (B/SBS/BW30) and 40 wt% BW (B/SBS/BW40). These two binders were prepared with the same B/SBS mass ratio of 7.33 which corresponds to the reference commercial B/SBS sample containing 12 wt % SBS (modified bituminous binder typically used in roofing industry). Thus, this test gives valuable information about the capacity of the created SBS network in the bituminous matrix to hold the maximum amount of beeswax during its melting process and, thereby to manufacture form-stable bituminous PCM binders. After processing, a portion of each ternary blend on a filter paper was placed in an oven at 80 °C (a temperature higher than BW melting temperature) for 5 days, and the digital photographs after the leakage tests conducted on binders are illustrated in Fig. S8 of the Supporting Information.

In addition, the standard allows to quantify the leakage rate (L) as the arithmetic mean of the four measurements of the exudate circle (each 45°) minus the inner diameter of the ring (16 mm) and divided by 2. It can be observed that, just after processing, B/SBS/BW30 binder presents some traces of exuded BW (L = 2.1 ± 0.6 mm), which is much lower than the massive exudate noticed for the ternary binder containing 40 wt% BW (L = 28.9 ± 1.9 mm). Interestingly, a value of L = 2.7 ± 0.5 mm is obtained when B/SBS/BW30 binder was previously subjected to 100 heating/cooling cycles (its corresponding digital photograph is included in Fig. S9 of the Supporting Information). Therefore, B/SBS/BW30 binder shows excellent long-term stability. Thus, since $T_{R\&B}$ value is associated to the breakdown of the SBS network (i.e., with the integrity of polymeric structure that below a critical point would not prevent BW leakage), binders with higher $T_{R\&B}$ values exhibit better leakproof performance, as corroborated B/SBS/BW30 and B/SBS/BW40 binders (with values of 102 and 89 °C, respectively). Therefore, for the selected B/SBS mass ratio of 7.33 (which is equivalent to the reference binary B/SBS binder), leakage tests would limit the maximum BW concentration to manufacture form-stable ternary blends to 30 wt%. Interestingly, B/SBS/BW30 binder also meets the $T_{R\&B}$ and P values required by Standard ASTM D8051, as seen in Fig. 6. In this sense, B/SBS binder (this is, a binary binder prepared with 12 wt% SBS) shows a high $T_{R\&B}$ value (113 °C) due to the formation of a continuous SBS network throughout the binder [44]. Thus, when 30 wt% BW melts during ring and ball softening test, $T_{R\&B}$ value slightly decreases from 113 °C, for B/SBS sample, to 102 °C for B/SBS/BW30 binder, which would indicate that this ternary binder also exhibits a continuous SBS network

Table 2
Thermal characteristics of BW, binary B/BW blends, and a selected ternary blend (B/SBS/BW30) after 1, 100 and 300 thermal cycles.

	ΔH_c (J/g)	$T_{c,o}$ (°C)	$T_{c,p}$ (°C)	ΔH_m (J/g)	$T_{m,o}$ (°C)	$T_{m,p}$ (°C)	η (%)
BW	175.68 ± 0.4	61.04 ± 0.2	56.14 ± 0.6	176.66 ± 0.6	48.56 ± 0.6	63.04 ± 0.5	–
B/BW10	16.68 ± 0.6	45.26 ± 0.4	39.52 ± 0.5	16.90 ± 0.5	30.77 ± 0.5	53.47 ± 0.8	95.7 ± 0.3
B/BW20	34.12 ± 0.5	50.48 ± 0.4	46.04 ± 0.6	35.92 ± 0.8	35.57 ± 0.6	55.26 ± 0.7	96.5 ± 0.4
B/BW30	50.18 ± 0.9	53.11 ± 0.5	49.02 ± 0.9	50.66 ± 0.9	39.83 ± 0.4	57.29 ± 0.7	95.6 ± 0.6
B/BW40	66.40 ± 0.9	54.72 ± 0.6	50.76 ± 0.7	66.78 ± 0.7	41.92 ± 0.5	59.04 ± 0.9	94.5 ± 0.5
B/SBS/BW30 (1-cycle)	50.15 ± 0.7	54.19 ± 0.7	47.29 ± 0.8	50.14 ± 0.5	39.32 ± 0.6	59.44 ± 0.4	94.6 ± 0.7
B/SBS/BW30 (100-cycle)	50.58 ± 0.5	54.37 ± 0.6	47.75 ± 0.7	50.61 ± 0.8	39.39 ± 0.3	59.34 ± 0.6	95.5 ± 0.5
B/SBS/BW30 (300-cycle)	50.92 ± 0.8	54.77 ± 0.5	47.62 ± 0.4	51.11 ± 0.7	39.42 ± 0.4	59.38 ± 0.6	96.4 ± 0.4

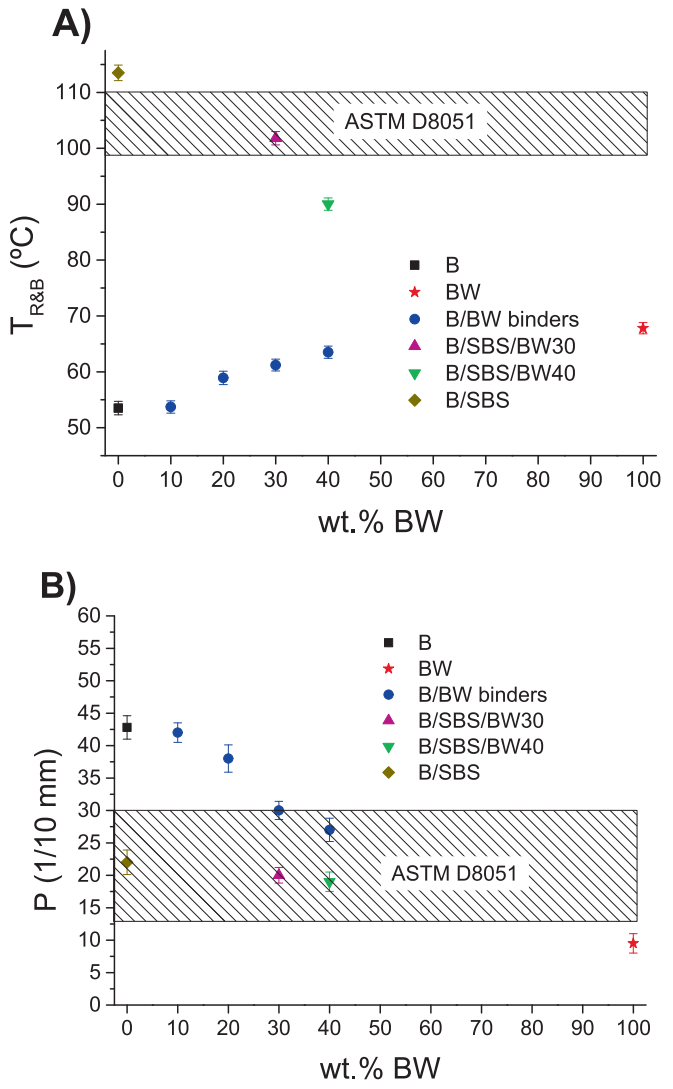

Fig. 6. A) Ring-and-ball softening temperature and B) penetration values for bitumen, beeswax and bituminous blends.

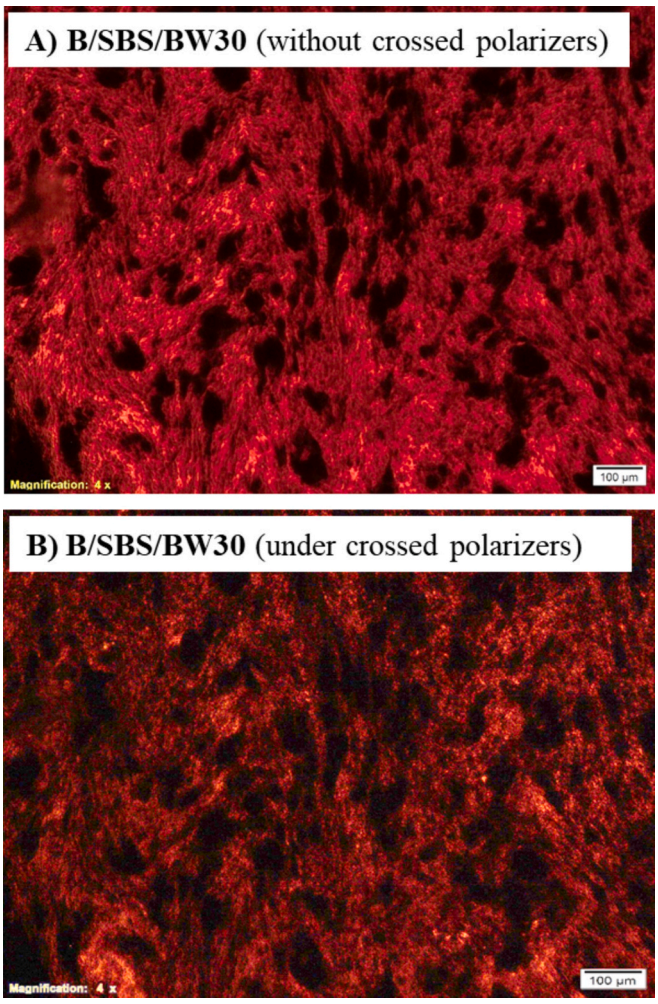

Fig. 7. Micrographs, taken at 25 °C, for ternary B/SBS/BW30 blend.

(polymer-rich phase) controlling the binder performance at high temperatures, as will be discussed below. In fact, this microstructure can be clearly deduced from the micrograph taken without crossed polarizers included in Fig. 7A, where the SBS-rich phase appears as light red zones and the bitumen-rich one as dark regions. In addition, the same micrograph taken under crossed polarizers (Fig. 7B, which allow BW crystals to be detected, revealed that these crystals are visible together with the polymeric SBS-rich phase of the binder. This fact is ascribed to the partial compatibility of some bitumen compounds and the amorphous BW phase [32].

Therefore, the results so far indicate that the ternary blend formulated with 30 wt% BW (B/SBS/BW30) is a form-stable bituminous binder that meet with the technological requirements established by Standard ASTM D8051 to be used for roofing applications.

With respect to the thermomechanical performance, temperature sweep tests in oscillatory shear were conducted on bitumen, binary B/BW30 binder and ternary B/SBS/BW30 sample. Fig. 8 displays the evolution of complex modulus |G*| (stiffness and overall resistance to deformation) between 30 and 80 °C for these samples. The same evolution with temperature follows the complex viscosity η*, since $\eta^* = |G^*| / \omega$ (where ω is the angular frequency and takes a constant value of 10 rad/s). As can be observed in Fig. 8, all binders undergo a decrease in |G*| with increasing testing temperature; however, notable differences

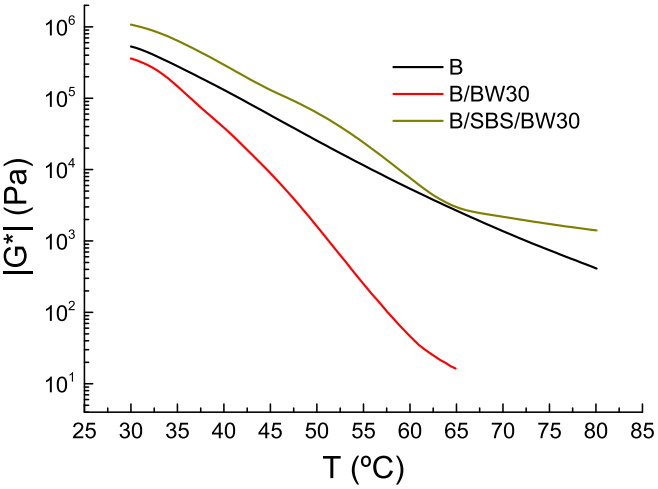

Fig. 8. Evolution of complex modulus with testing temperature for base bitumen, binary B/BW30 binder and ternary B/SBS/BW30 sample.

among samples can be found that deserve to be analysed. On the one hand, base bitumen shows a steady fall of |G*| with testing temperature, which is indicative of its direct transition from glassy to the Newtonian region. On the other hand, after adding 30 wt% BW to base bitumen, the corresponding binary B/BW30 sample exhibits lower |G*| values than

bitumen due to BW melting over the entire testing temperature range. According to the DSC profile of BW, this effect is much more pronounced as testing temperature increases, which indicates a considerable worsening in its mechanical response. As for the ternary B/SBS/BW30 binder, the continuous SBS network created plays a decisive role in the thermomechanical performance. Thus, this binder displays a two-step decay process of |G*| characterized by a decrease stage, being more pronounced in the range between 50 and 60 °C, reaching a flattening of the slope at ca. 65 °C. This enhancement in the mechanical response at high temperatures is attributed to the viscosity of the bitumen being low enough to allow the elastic network of SBS to influence the mechanical properties of the ternary blend [31]. Therefore, the creation of a continuous SBS network throughout the binder is essential not only to avoid PCM leakage but also to improve the thermomechanical properties especially at high in-service temperatures.

Next, the thermal stability of this selected binder was evaluated by thermogravimetric analysis (TGA). Fig. 9 displays the weight loss and its derivative (DTG) for B/SBS/BW30 blend and its parent components (B, BW and SBS) for the sake of comparison.

As for parent components, different TGA thermograms are observed: i) one the one hand, SBS and BW display one single degradation step (with their maximum rate at 454 and 401 °C, respectively) without no char residues detected; ii) on the other hand, B sample shows a wide temperature range decomposition composed of two overlapped events (with the maximum rate located at 453 °C, similar to SBS sample) and a residue content of 14.7 wt%. As expected, B/SBS/BW30 binder displays the two thermal decomposition stages corresponding to the simultaneous decomposition of B and SBS, and that for BW. From a point of view of its processing and potential application, the ternary prototype here considered presents excellent thermal stability, since there is no weight loss either in the temperature range suitable for solar energy collection (<65 °C) or at the high processing temperature (typically, 180 °C) used for the manufacture of bitumen-based roofing materials [45].

In addition to thermal stability, the selected ternary binder should present adequate thermal storage capacity for a long-time period to be used as roofing materials. To explore this, a DSC thermal cycling test consisted in repeated melting and crystallization cycles (up to 300 heating/cooling scans) was conducted on B/SBS/BW30 binder, and its DSC curves and corresponding thermal characteristics are gathered in Fig. 10 and Table 2.

As can be observed, DSC curves after 1, 100 and 300 heating/cooling cycles are totally coincident, ant thereby so are the characteristic temperatures and enthalpies. Consequently, B/SBS/BW30 binder exhibits adequate thermal cycling reliability after long-term utility period. In addition, the selected binder shows a thermal storage capacity of 50 J/g which, besides being in line with other bio-based PCM building materials [21], is a suitable value to produce energy savings in buildings [46].

In order to more realistically measure the thermal storage capacity of the selected ternary blend, indoor thermoregulation tests in a climatic chamber were conducted following the experimental setup described in subsection 2.3.5 and expanded in the Supporting Information. Thus, the prototype B/SBS/BW30 binder was integrated as roofing material in a reduced-scaled isolated room and was subsequently subjected to an incident radiation of 1000 ± 25 W/m^2 for 90 min while the surrounding air (T_{su}) is kept at 27.5 ± 1.0 °C. To be used as reference, the commercial B/SBS bituminous binder (typically used in the roofing industry) was also subjected to the same thermoregulation test. Fig. 12 plots the temperature–time curve of the uppermost (T_{up}) and lowermost (T_{up}) surface of the roofing material, the surrounding air (T_{su}), and the air inside the isolated room (T_{in}) for these two roofing materials. As commented in the Supporting Information, it is important to note that before starting the thermoregulation test and the roofing material is irradiated with 1000 ± 25 W/m^2, sample was subjected to a 4-hour preconditioning period in which was irradiated with 60 W/m^2 until all temperatures are equilibrated. Thus, during this preliminary stage there

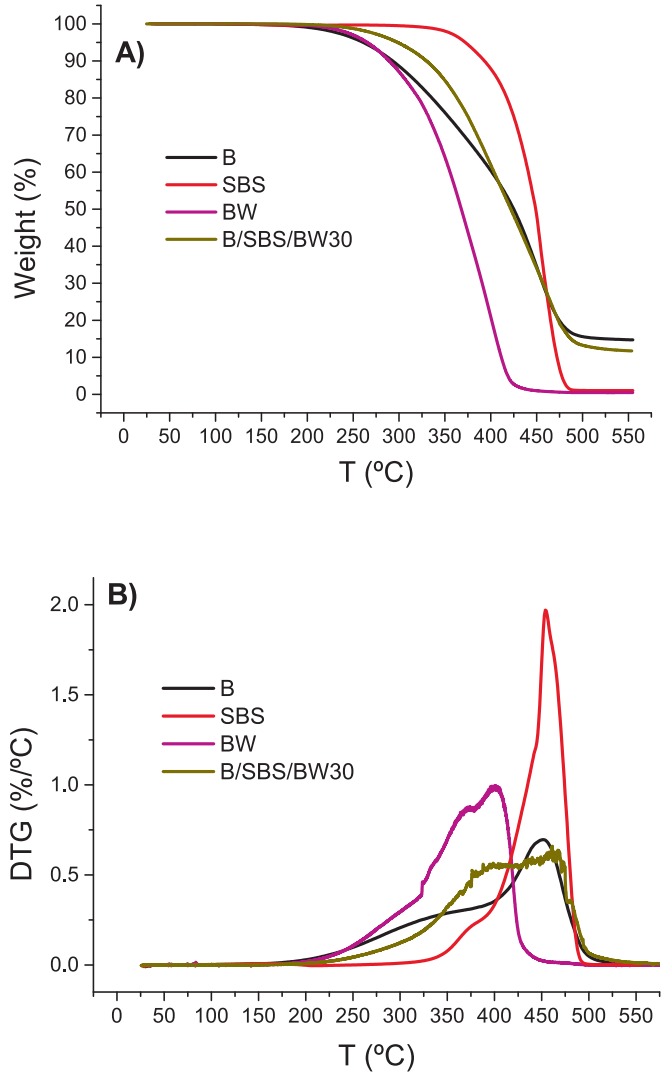

Fig. 9. A) Weight loss and B) its derivative (DTG) for bitumen (B), beeswax (BW), SBS and the ternary B/SBS/BW30 blend.

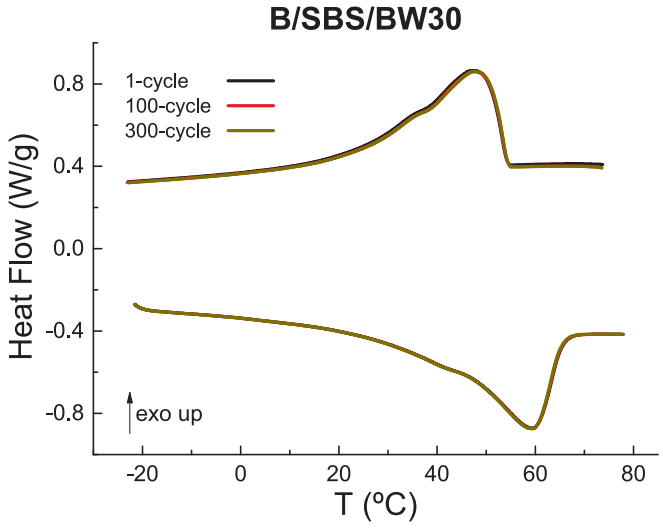

Fig. 10. DSC heating and cooling scans of ternary B/SBS/BW30 blend after 1, 100 and 300 thermal cycles.

is a slight heat flux into the room that causes starting values following the order $T_{up} > T_{lo} > T_{in}$ in the thermoregulation test illustrated in Fig. 11.

During the indoor thermoregulation test, the roofing material received a simulated solar irradiation of 1000 ± 25 W/m^2 on its uppermost surface of which a part is absorbed and the heat is conducted throughout the material to the inside of the room, and the rest is reflected, emitted as heat radiation and lost by free convection. Considering the low thermal conductivity of the XPS (0.030 W/m°C) and the large thickness of the foam walls, a one-dimensional heat transfer into the room can be assumed. As seen in Fig. 11, whereas the surrounding air (T_{su}) is kept at 27.5 ± 1.0 °C, the evolution of the uppermost surface temperature (T_{up}) over irradiation time is characterized by an initial rapid rise and a subsequent tendency to reach the equilibrium. A similar pattern is also noticed for the lowermost surface (T_{lo}) and the temperature of the air inside the room (T_{in}), although with a less pronounced temperature increase, respectively. Interestingly, the thermoregulation ability of the prototype B/SBS/BW30 is clearly noted by comparing its temperature vs. time curves with those for the reference B/SBS sample. Thus, as the temperature of the B/SBS/BW30 roofing material increases (from T_{lo} and T_{up} values of ca. 30 and 31 °C, respectively, up to ca. 56 and 60 °C) its beeswax progressively melts to absorb the solar-thermal energy and stored it in the way of latent heat [47]. This fact is reflected in lower initial heating rates for the B/SBS/BW30 binder compared to the reference B/SBS sample.

In addition to that, the heat needed to be removed from the room to keep it at a desired indoor temperature (T_{de}) of 25 °C when acting as roofing material the reference B/SBS binder or the prototype B/SBS/BW30 blend can be calculated by Eqs. (2) and (3), respectively [48]:

$$Q_{B/SBS} = \int_{t=0}^{t_{final}} m_{air} \cdot Cp_{air} \cdot (T_{in}|_{B/SBS} - T_{de}) dt \quad (2)$$

$$Q_{B/SBS/BW30} = \int_{t=0}^{t_{final}} m_{air} \cdot Cp_{air} \cdot (T_{in}|_{B/SBS/BW30} - T_{de}) dt \quad (3)$$

where m_{air} and Cp_{air} are the air mass contained in the room and its specific heat capacity, respectively; t_{final} is the final time of the thermoregulation tests (ca. 90 min); $T_{in}|_{B/SBS}$ and $T_{in}|_{B/SBS/BW30}$ are the temperature of the air inside the room when acting B/SBS or B/SBS/BW30 as roofing material, respectively; and T_{de} is the desired indoor temperature (which was fixed at 25 °C). For the same desired indoor temperature (T_{de}) of 25 °C, the required energy for air conditioning

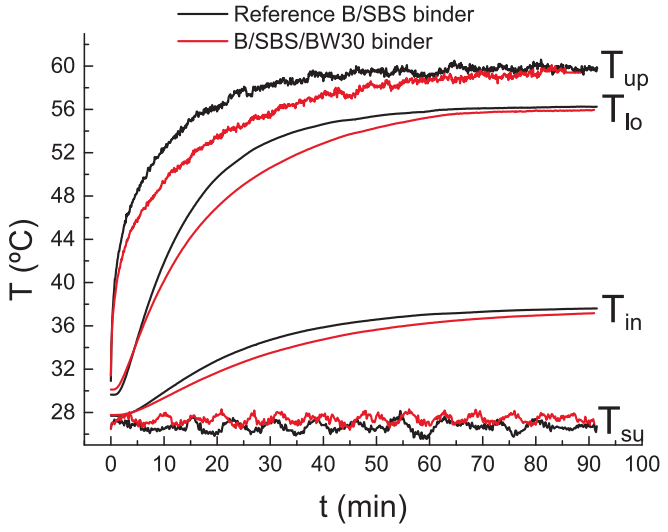

Fig. 11. Temperature-time curve of the different temperature sensors for the commercial bituminous B/SBS sample and the prototype B/SBS/BW30 binder.

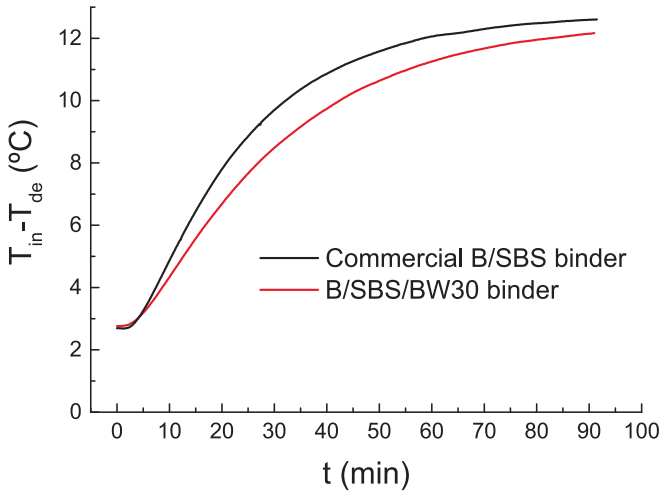

Fig. 12. Evolution with time of the difference between the temperature of the air inside the room (T_{in}) and the desired indoor temperature (T_{de}) of 25 °C for the commercial bituminous B/SBS sample and the prototype B/SBS/BW30 binder.

inside the room would be reduced if the difference between the temperature of the air inside the room (T_{in}) and the T_{de} was less.

Thus, the percentage reduction (Ω) in the heat needed to be removed from the room during the thermoregulation test when comparing the prototype B/SBS/BW30 binder with the commercial B/SBS sample is calculated as follows:

$$\Omega = \left(1 - \frac{Q_{B/SBS/BW30}}{Q_{B/SBS}}\right) \cdot 100 = \left(1 - \frac{\int_{t=0}^{t_{final}} (T_{in}|_{B/SBS/BW30} - T_{de}) dt}{\int_{t=0}^{t_{final}} (T_{in}|_{B/SBS} - T_{de}) dt}\right) \cdot 100 \quad (4)$$

The graphic integration of the corresponding $T_{in} - T_{de}$ vs. time curves from Fig. 12 yields a percentage reduction (Ω) of 9.3 %.

Finally, Table 3 gathers the density at 25 °C ($\rho_{25°C}$) and thermal conductivity at 45 °C ($k_{45°C}$) for the reference bituminous B/SBS sample and the proposed B/SBS/BW30 binder.

The insulation capacity of roofing materials improves as their density and thermal conductivity decrease. As seen in Table 3, B/SBS/BW30 presents a slightly lower density value than the reference B/SBS binder. As for thermal conductivity, on the one hand, the addition of 30 wt% BW results in a increase in the thermal conductivity for B/SBS/BW30 binder, which is attributed to the higher thermal conductivity of BW (0.248 ± 0.002) compared to base bitumen (0.149 ± 0.003), a fact that would reduce its insulation capacity. However, on the other hand, the thermal conductivity of a thermal energy storage material must be sufficiently large to facilitate heat transfer and thus promote use of the full thermal storage capacity of the material [49]. Thus, although thermal conductivity is an important parameter in determination of the heat storage and release characteristics of the thermal energy storage materials, the melting temperature and latent heat capacity are the most critical limiting factors for implementation into building applications [46]. Therefore, beeswax represents a promising, eco-conscious PCM alternative, facilitating both waste reduction and the development of sustainable energy technologies, to manufacture energy-efficient roofing materials for building applications.

Table 3
Density at 25 °C ($\rho_{25°C}$) and thermal conductivity at 45 °C ($k_{45°C}$) of reference B/SBS sample and the proposed B/SBS/BW30 binder.

	$\rho_{25°C}$ (g/cm^3)	$k_{45°C}$ (W/m°C)
B/SBS	1.018 ± 0.005	0.155 ± 0.002
B/SBS/BW30	1.002 ± 0.003	0.179 ± 0.001

4. Concluding remarks

Form-stable ternary bitumen(B)/polymer(SBS)/beeswax(BW) binders were successfully manufactured to be applied as energy-efficient roofing materials. Since non-encapsulated BW was used as bio-based PCM, the effects of possible interactions between B compounds and BW on thermal storage capacity and technological characterization were firstly evaluated on binary B/BW blends. DSC results revealed relative enthalpy efficiency (η) values around 96 % which indicates that most of the crystalline structure of BW is retained in the blends and, thereby the latent heat capacity of BW is only weakly reduced. However, the softening temperatures of these binary B/BW blends are far from those specified by ASTM D8051 for wax-modified asphaltic roofing products even for a BW concentration of 40 wt%. Aiming to enhance the high temperature performance and to prevent BW leakage, a polymer (SBS) was included in the blend formulation to create a well-developed SBS network in the bitumen-rich phase. Leakage tests conducted on B/SBS/BW blends prepared at a fixed B/SBS mass ratio of 7.33 (which corresponds to the commercial B/SBS sample containing 12 wt% SBS typically used in roofing industry) indicated that the maximum BW content to avoid its leakage is 30 wt%. Interestingly, the prototype roofing material (composed of 61.6 wt% B, 8.4 wt% SBS and 30 wt% BW) meets the technological requirements (ring-and-ball softening point and penetration) specified by ASTM D8051, since the continuous SBS network observed by optical microscopy controls the binder performance at high temperatures. In addition, this prototype shows excellent thermal stability (no weight loss up to ca. 200 °C) and high thermal storage capacity (ca. 50 J/g, in line with other bio-based PCM building materials) for a long period of time (at least, for 300 heating/cooling cycles). Finally, this binder was integrated as roofing material in a reduced-scaled isolated room, and was subjected to an incident radiation of 1000 ± 25 W/m^2 for 90 min while the surrounding air is kept at 27.5 ± 1.0 °C in a climatic chamber. The percentage reduction in the heat needed to be removed from the room when comparing the prototype B/SBS/BW30 binder with the commercial B/SBS binder was 9.3 %, which makes beeswax a promising bio-based PCM to manufacture energy-efficient roofing materials for warm climates. To sum up, it is considered that future actions should be directed towards (i) selecting bio-PCMs with lower transition temperatures that extend their use beyond warm climates, and (ii) using new polymer supporting materials that allow us to manufacture form-stable thermal storage energy materials with higher bio-PCM content.

CRediT authorship contribution statement

E. Álvarez-Gallardo: Writing – original draft, Methodology, Investigation. **A. Tenorio-Alfonso:** Writing – review & editing, Writing – original draft, Methodology, Investigation, Conceptualization. **A.A. Cuadri:** Writing – review & editing, Writing – original draft, Supervision, Project administration, Methodology, Investigation, Funding acquisition, Conceptualization.

Funding

This work is part of the project PID2023-149701OA-I00 funded by MCIN/AEI/10.13039/501100011033 (Spanish Ministry of Science, Innovation and Universities) and ERDF "A way of making Europe". Funding for open access charge: Universidad de Huelva / CBUA.

Declaration of competing interest

The authors declare that they have no known competing financial interests or personal relationships that could have appeared to influence the work reported in this paper.

Appendix A. Supplementary data

Supplementary data to this article can be found online at https://doi.org/10.1016/j.applthermaleng.2025.127617.

Data availability

The data that has been used is confidential.

References

[1] C. Alkan, E.H. Alakara, S.A. Aksoy, I. Demir, Cement mortar composites including 1-tetradecanol@PMMA Pickering emulsion particles for thermal energy management of buildings, Chem. Eng. J. 476 (2023) 146843, https://doi.org/10.1016/j.cej.2023.146843.
[2] Q. Al-Yasiri, M. Szabo, Incorporation of phase change materials into building envelope for thermal comfort and energy saving: a comprehensive analysis, J. Build. Eng. 36 (2021) 102122, https://doi.org/10.1016/j.jobe.2020.102122.
[3] M.H. Jahangir, M. Tarhani, K. Azadi, Comprehensive energy optimization in buildings using dual-layer PCM in different climates, Appl. Therm. Eng. 274 (2025) 126585, https://doi.org/10.1016/j.applthermaleng.2025.126585.
[4] R.K. Sharma, A. Kumar, D. Rakshit, A phase change material (PCM) based novel retrofitting approach in the air conditioning system to reduce building energy demand, Appl. Therm. Eng. 238 (2024) 121872, https://doi.org/10.1016/j.applthermaleng.2023.121872.
[5] V.J. Reddy, M.F. Ghazali, S. Kumarasamy, Advancements in phase change materials for energy-efficient building construction: a comprehensive review, J. Energy Storage 81 (2024) 110494, https://doi.org/10.1016/j.est.2024.110494.
[6] M. Álvarez-Rodríguez, M. Alonso-Martínez, I. Suarez-Ramon, P.J. García-Nieto, Numerical model for determining the effective heat capacity of macroencapsulated PCM for building applications, Appl. Therm. Eng. 242 (2024) 122478, https://doi.org/10.1016/j.applthermaleng.2024.122478.
[7] H.M. Ali, T. Rehman, M. Arıcı, Z. Said, B. Durakovic, H.I. Mohammed, R. Kumar, M.K. Rathod, O. Buyukdagli, M. Teggar, Advances in thermal energy storage: fundamentals and applications, Prog. Energy Combust. Sci. 100 (2024) 101109, https://doi.org/10.1016/j.pecs.2023.101109.
[8] R.M. Kalombe, S. Sobhansarbandi, J. Kevern, Assessment of low-cost organic phase change materials for improving infrastructure thermal performance, Constr. Build. Mater. 369 (2023), https://doi.org/10.1016/j.conbuildmat.2022.130285.
[9] X. ni Chen, B. Xu, Y. Fei, W. tao Gan, G. Pei, Parameter optimization of phase change material and the combination of phase change material and cool paint according to corresponding energy consumption characteristics under various climates, Energy 277 (2023), https://doi.org/10.1016/j.energy.2023.127625.
[10] T. Jiang, C. Zheng, S. You, H. Zhang, Z. Wu, Y. Wang, S. Wei, Experimental and numerical study on the heat transfer performance of the radiant floor heating condenser with composite phase change material, Appl. Therm. Eng. 213 (2022), https://doi.org/10.1016/j.applthermaleng.2022.118749.
[11] H.M. Abbas, J.M. Jalil, S.T. Ahmed, Experimental and numerical investigation of PCM capsules as insulation materials inserted into a hollow brick wall, Energ. Buildings 246 (2021), https://doi.org/10.1016/j.enbuild.2021.111127.
[12] P. Bébin, J. Fiset, L. Gagné, Octadecane filled bubble wrap as phase change material layers to smooth temperature variations of buildings during summer time. An experimental study, Energ. Buildings 277 (2022), https://doi.org/10.1016/j.enbuild.2022.112568.
[13] G. Polacco, J. Stastna, D. Biondi, L. Zanzotto, Relation between polymer architecture and nonlinear viscoelastic behavior of modified asphalts, Curr. Opin. Colloid Interface Sci. 245 (2006) 11230, https://doi.org/10.1016/j.cocis.2006.09.001.
[14] R. Aridi, A. Yehya, Review on the sustainability of phase-change materials used in buildings, Energy Conv. Manag-X 15 (2022) 100237, https://doi.org/10.1016/J.ECMX.2022.100237.
[15] S. Kahwaji, M.A. White, Edible oils as practical phase change materials for thermal energy storage, Appl. Sci. 9 (2019) 1627, https://doi.org/10.3390/app9081627.
[16] C.A. Saleel, A review on the use of coconut oil as an organic phase change material with its melting process, heat transfer, and energy storage characteristics, J. Therm. Anal. Calorim. 147 (2022) 4451–4472, https://doi.org/10.1007/s10973-021-10839-7.
[17] L. Boussaba, A. Foufa, S. Makhlouf, G. Lefebvre, L. Royon, Elaboration and properties of a composite bio-based PCM for an application in building envelopes, Construct. Build Mater. 185 (2018) 156–165, https://doi.org/10.1016/j.conbuildmat.2018.07.098.
[18] P. Jin Ong, et al., Valorization of Spent coffee Grounds: a sustainable resource for Bio-based phase change materials for thermal energy storage, Waste Manag. 157 (2023) 339–347, https://doi.org/10.1016/j.wasman.2022.12.039.
[19] N.D. Lorenzo, L.S. Kuhn, T.C. Guimaraes, M.N. Sam, C. Mankel, A. Caggiano, E. Koenders, C.A. Nunes, S.R. Ferreira, Potential use of bio-oleogel as phase change material, Sustainability 15 (2023) 2534, https://doi.org/10.3390/su15032534.
[20] I.M. Rasta, I.N. Suamir, The role of vegetable oil in water based phase change materials for medium temperature refrigeration, J. Energy Storage 15 (2018) 368–378, https://doi.org/10.1016/j.est.2017.12.014.
[21] F.F. de Alburquerque Landi, C. Fabiani, A.L. Pisello, Palm oil for seasonal thermal energy storage applications in buildings: the potential of multiple melting ranges in

blends of bio-based fatty acids, J Energy Storage 29 (2020) 101431, https://doi.org/10.1016/j.est.2020.101431.
[22] C. Fabiani, A.L. Pisello, M. Barbanera, L.F. Cabeza, Palm-oil bio-PCM for energy efficient building applications: Multipurpose thermal investigation and life cycle assessment, J. Energy Storage 28 (2020) 101129, https://doi.org/10.1016/j.est.2019.101129.
[23] L. Boussaba, S. Makhlouf, A. Foufa, G. Lefebvre, L. Royon, Vegetable fat: a low-cost bio-based phase change material for thermal energy storage in buildings, J. Build. Eng. 21 (2019) 222–229, https://doi.org/10.1016/J.JOBE.2018.10.022.
[24] S.B. Belgacem, A. Trigui, I. Jedidi, M.S. Loukil, M. Calmunger, M. Abdomouleh, Enhancing thermal energy storage properties of blend phase change materials using beeswax, Environ. Sci. Pollut. Res. 31 (2024) 51504–51520, https://doi.org/10.1007/s11356-024-34591-1.
[25] P.K.S. Rathore, K.K. Gupta, B. Patel, R.K. Sharma, N.K. Gupta, Beeswax as a potential replacement of paraffin wax as shape stabilized solar thermal energy storage material: an experimental study, J. Energy Storage 68 (2023) 107714, https://doi.org/10.1016/j.est.2023.107714.
[26] R. Thaib, M. Amin, H. Umar, Thermal properties of beef tallow/coconut oil bio PCM using T-history method for wall building applications, Eur. J. Eng. Res. Sci. 4 (2019) 38–40. https://doi.org/10.24018/ejeng.2019.4.11.1627.
[27] S.G. Jeong, S. Wi, S.J. Chang, J. Lee, S. Kim, An experimental study on applying organic PCMs to gypsum-cement board for improving thermal performance of buildings in different climates, Energy Build. 190 (2019) 183–194, https://doi.org/10.1016/j.enbuild.2019.02.037.
[28] A. Dinker, M. Agarwal, G.D. Agarwal, Experimental assessment on thermal storage performance of beeswax in a helical tube embedded storage unit, Appl. Therm. Eng. 111 (2017) 358–368, https://doi.org/10.1016/J.APPLTHERMALENG.2016.09.128.
[29] F.J. Ortega, F.J. Navarro, M. García-Morales, T. McNally, Thermo-mechanical behaviour and structure of novel bitumen/nanoclay/MDI composites, Compos. Pt. B-Eng. 76 (2015) 192–200, https://doi.org/10.1016/j.compositesb.2015.02.030.
[30] M.J. Martín-Alfonso, P. Partal, F.J. Navarro, M. García-Morales, C. Gallegos, Use of MDI-functionalized reactive polymer for the manufacture of modified bitumen with enhanced properties for roofing applications, Eur. Polym. J. 44 (2008) 1451–1461, https://doi.org/10.1016/j.eurpolymj.2008.02.026.
[31] G.D. Airey, Rheological properties of styrene butadiene styrene polymer modified road bitumens, Fuel 82 (2003) 1709–1719, https://doi.org/10.1016/S0016-2361(03)00146-7.
[32] A.A. Cuadri, C. Delgado-Sánchez, A. Tenorio-Alfonso, P. Partal, F.J. Navarro, Form-stable bitumen/paraffin-wax/polymer binders for energy-efficient building applications, J. Energy Storage 93 (2024) 112420, https://doi.org/10.1016/j.est.2024.112420.
[33] C. Delgado-Sánchez, E. Cortés-Triviño, A. Tenorio-Alfonso, F.J. Navarro, Innovative stearic acid-in-silicone oil (o/o) phase change material lubricating emulsions (PCMLEs): thermo-rheological and tribological properties, J. Mol. Liq. 399 (2024) 124481, https://doi.org/10.1016/j.molliq.2024.124481.
[34] A. Bucio, R. Moreno-Tovar, L. Bucio, J. Espinosa-Dávila, F. Anguebes-Franceschi, Characterization of beeswax, candelilla wax and paraffin wax for coating cheeses, Coatings 11 (2021) 261, https://doi.org/10.3390/coatings11030261.
[35] K. Pielichowska, K. Pielichowski, Phase change materials for thermal energy storage, Prog. Mater Sci. 65 (2014) 67–123, https://doi.org/10.1016/j.pmatsci.2014.03.005.
[36] B. Li, S. Stüwe, J. Mirwald, B. Hofko, Characterizing the diversity of PmB aging with application to pavements, Fuel 400 (2025) 135803, https://doi.org/10.1016/j.fuel.2025.135803.
[37] X. Lu, P. Redelius, Compositional and structural characterization of waxes isolated from bitumens, Energy Fuels 20 (2006) 653–660, https://doi.org/10.1021/ef0503414.
[38] J. Wang, M.D. Calhoun, S.J. Severtson, Dynamic rheological study of paraffin wax and its organoclay nanocomposites, J. Appl. Polym. Sci. 108 (2008) 2564–2570, https://doi.org/10.1002/app.27768.
[39] C. Gutiérrez-Blandón, A.A. Cuadri, A. Tenorio-Alfonso, P. Partal, F.J. Navarro, Rheological and phase behaviour of paraffin wax/bitumen blends with thermal storage characteristics, Constr. Build. Mater. 401 (2023) 132826, https://doi.org/10.1016/j.conbuildmat.2023.132826.
[40] C. Gutiérrez-Blandón, A.A. Cuadri, P. Partal, A. Tenorio-Alfonso, C. Delgado-Sánchez, F.J. Navarro, Rheological aspects of solid-to-liquid phase transitions in paraffin wax/bitumen blends for thermal energy storage applications, Appl. Therm. Eng. 253 (2024) 123779, https://doi.org/10.1016/j.applthermaleng.2024.123779.
[41] C. Gutiérrez-Blandón, A.A. Cuadri, C. Delgado-Sánchez, P. Partal, F.J. Navarro, Study on miscibility, thermomechanical behavior, and thermoregulation performance of paraffin wax/bituminous blends for solar thermal energy storage applications, Energy Fuels 38 (2024) 3407–3416, https://doi.org/10.1021/acs.energyfuels.3c04229.
[42] K. Du, J. Calautit, Z. Wang, Y. Wu, H. Liu, A review of the applications of phase change materials in cooling, heating and power generation in different temperature ranges, Appl. Energy 220 (2018) 242–273, https://doi.org/10.1016/j.apenergy.2018.03.005.
[43] K.Y. Leong, S. Hasbi, K.Z.K. Ahmad, N.M. Jali, H.C. Ong, M.F.M. Din, Thermal properties evaluation of paraffin wax enhanced with carbon nanotubes as latent heat thermal energy storage, J. Energy Storage 52 (2022) 105027, https://doi.org/10.1016/j.est.2022.105027.
[44] O.V. Laukkanen, H. Soenen, H.H. Winter, J. Seppälä, Low-temperature rheological and morphological characterization of SBS modified bitumen, Constr. Build. Mater. 179 (2018) 348–359, https://doi.org/10.1016/j.conbuildmat.2018.05.160.
[45] W. Kong, Z. Liu, Y. Yang, C. Zhou, J. Lei, Preparation and characterizations of asphalt/lauric acid blends phase change materials for potential building materials, Constr. Build. Mater. 152 (2017) 568–575, https://doi.org/10.1016/j.conbuildmat.2017.05.039.
[46] C. Baylis, C.A. Cruickshank, Review of bio-based phase change materials as passive thermal storage in buildings, Renew. Sust. Energ. Rev. 186 (2023) 113690, https://doi.org/10.1016/j.rser.2023.113690.
[47] J. Huang, Y. Liu, J. Lin, J. Su, C. Redshaw, X. Feng, Y. Min, Novel pyrene-based aggregation-induced emission luminogen (AIEgen) composite phase change fibers with satisfactory fluorescence anti-counterfeiting, temperature sensing, and high-temperature warning functions for solar-thermal energy storage, Adv. Compos. Hydrid Mater. 6 (2023) 126, https://doi.org/10.1007/s42114-023-00706-4.
[48] H.M. Chou, C.R. Chen, V.L. Nguyen, A new design of metal-sheet cool roof using PCM, Energy Build. 57 (2013) 42–50, https://doi.org/10.1016/j.enbuild.2012.10.030.
[49] L. Fan, J.M. Khodadadi, Thermal conductivity enhancement of phase change materials for thermal energy storage: a review, Renew. Sustain. Energy Rev. 15 (2011) 24–46, https://doi.org/10.1016/j.rser.2010.08.007.